Effects of disorder and hydrostatic pressure on charge density wave and superconductivity in $2H$-TaS$_2$

Shuxiang Xu [1,2,*] Jingjing Gao,[3,4,*] Ziyi Liu,[1] Keyu Chen,[1,2] Pengtao Yang,[1] Shangjie Tian [5] Chunsheng Gong,[5] Jianping Sun [1,2] Mianqi Xue,[6] Jun Gouchi,[7] Xuan Luo,[3,†] Yuping Sun,[3,8,9] Yoshiya Uwatoko,[7] Hechang Lei,[5,‡] Bosen Wang,[1,2,10,§] and Jinguang Cheng [1,2]

[1]*Beijing National Laboratory for Condensed Matter Physics and Institute of Physics,*
Chinese Academy of Sciences, Beijing 100190, China
[2]*School of Physical Sciences, University of Chinese Academy of Sciences, Beijing 100190, China*
[3]*Key Laboratory of Materials Physics, Institute of Solid State Physics, Chinese Academy of Sciences, Hefei 230031, China*
[4]*Science Island Branch of Graduate School, University of Science and Technology of China, Hefei 230026, China*
[5]*Department of Physics and Beijing Key Laboratory of Opto-electronic Functional Materials & Micro-nano Devices,*
Renmin University of China, Beijing 100872, China
[6]*Technical Institute of Physics and Chemistry, Chinese Academy of Sciences, Beijing 100190, China*
[7]*Institute for Solid State Physics, University of Tokyo, Kashiwanoha 5-1-5, Kashiwa, Chiba 277–8581, Japan*
[8]*High Magnetic Field Laboratory, Chinese Academy of Sciences, Hefei 230031, China*
[9]*Collaborative Innovation Center of Microstructures, Nanjing University, Nanjing 210093, China*
[10]*Songshan Lake Materials Laboratory, Dongguan, Guangdong 523808, China*

We report the comparative effects of disorder and hydrostatic pressure on charge density wave (CDW) and superconductivity (SC) in $2H$-TaS$_2$ by measuring electrical resistivity and ac magnetic susceptibility. For the crystals in the clean limit (low disorder level), CDW ground state is suppressed completely at a critical pressure $P_c \sim 6.24(5)$ GPa where a dome-shaped pressure dependence of superconducting transition temperature $T_c(P)$ appears with a maximum value of $T_c^{max} \sim 9.15$ K, indicating strong competitions between CDW and SC. The temperature exponent n of low-temperature resistivity data decreases from ~ 3.36 at ambient pressure (AP) to $\sim 1.29(2)$ at P_c and then retains a saturated value $\sim 2.10(4)$ when the pressure is higher than 7.5 GPa; accordingly, the quadratic temperature coefficient of normal-state resistivity A peaks out just at P_c with an enhancement by nearly one order in magnitude. These features strongly manifest that the enhanced critical CDW fluctuations near P_c are possible important glues for superconducting pairings. High-pressure magnetic susceptibility indicates that superconducting shielding volume increases with pressure and retains a nearly constant value above P_c, which evidences that the enhancement of $T_c(P)$ is accompanied by the expense of CDW. For those crystals in dirty limit (high disorder level), there is no clear CDW phase transition in resistivity; the pressure dependence of $T_c(P)$ and n broadens up and becomes less apparent in comparison with the clean crystals. Our results suggest that disorder scattering and the melting of CDW are two factors affecting SC, and the melting of CDW dominates the change of T_c below P_c; the enhancement of $T_c(P)$ is associated with the suppression of CDW by pressure and the increase in the density of states at Fermi level; however, after the CDW collapse, superconducting pairing strength is strongly weakened by impurity scattering above P_c according to Anderson's theorem.

I. INTRODUCTION

The interplay of charge density wave (CDW) and superconductivity (SC) has received continuous and considerable attention over the past decades [1,2]. On one hand, it can provide excellent opportunities to explore new superconducting materials considering cooperation and competition of CDW and SC; superconductivity can be realized frequently through element doping and applying physical pressure which effectively suppress the CDW ground state of materials [3–7]. On the other hand, previously reported phase diagrams concerning the evolution of CDW and SC often exhibit distinct characteristics which strongly depend on the external parameters [3,6,8,9]. In some typical quasi-two-dimensional CDW materials such as $2H$-Ta(Se, S)$_2$, it was argued that a superconducting state can coexist with long-range CDW order in real space [6,7]; contrarily, CDW and SC are mutually exclusive without any pressure overlap in phase diagrams of other CDW materials, for example, $1T$-Ta(Se, S)$_2$ and $1T$-TiSe$_2$ [3,8–10]. It is thought that difference band structures caused by slightly change of crystal symmetry is one of critical factors. However, in both cases, some short-range CDW order that may be undetectable in electrical transport

---
[*]The first two authors contributed equally.
[†]Corresponding author: xluo@issp.ac.cn
[‡]Corresponding author: hlei@ruc.edu.cn
[§]Corresponding author: bswang@iphy.ac.cn

properties would still coexist with SC after further collapse of CDW order [3,9,11]. It usually involves whether electronic states responsible for superconducting pairing and CDW formation comes from the same pockets of Fermi surfaces and possible interband couplings [2,12–14]. These characteristics also reflect the complicated interplay of CDW and SC [3,6–10]. So far, there is still no widely acceptable explanation for the changes of T_c in various CDW materials. And more studies on phase diagrams of CDW and SC for various CDW materials can deepen our understandings on these scientific issues.

As typical CDW materials, layered transition-metal dichalcogenides (TMDCs) have been widely studied [5–10]. Among them, $2H$-TaS_2 is one special case showing only one CDW phase transition at ambient pressure (AP), different from the multi-CDWs in other TMDCs materials [1]. It transforms from an ordinary metallic phase into a 3×3 incommensurate CDW (ICCDW) state at $T_{ICCDW} \sim 78$ K, prior to the emergence of bulk superconducting state at the superconducting transition temperature $T_c \sim 0.8$ K [15]. Recently, $2H$-TaS_2 was hotly concerned and studied owing to large divergences in superconducting diagrams under pressure [16–20]. At first, Freitas *et al.* reported a pressure-induced strong enhancement of T_c from temperatures below 1 K up to 8.50 K at 9.50 GPa in $2H$-TaS_2 [16]; however, ICCDW phase transition is robust against pressure and can persist up to at least 17 GPa. The coexistence of CDW and SC cannot be understood easily without magnetic susceptibility under pressures [16]. In contrast, Grasset *et al.* argued that the collapse of CDW order takes place around a much lower critical pressure $P_c \sim 8.50$ GPa where the Higgs model, which is thought to be closely associated with a strong in-gap superconducting mode, vanishes, and a superconducting state exists above P_c [17]. And then, the pressure-induced collapse of CDW was verified by measuring Raman scattering and electrical resistivity in a diamond anvil pressure cell; the critical pressure P_c is about 7.30 GPa but T_c increases with increasing pressure and reaches a maximum of 9.15 K at 11.5 GPa [18]. In a recent work, CDW was reported to be completely suppressed at a critical pressure $P_c \sim 8.70$ GPa with a domelike pressure dependence of T_c; first-principles calculations reveal that the suppression of CDW is closely associated with distorted lattice and phonon instability under pressure [19]. From these results, it may be seen that superconducting phase diagrams strongly depend on pressure environments and sample qualities [8]. As we know, element doping, Cu intercalation, and physical pressure are effective methods to tune the interplay of CDW and SC, but the resultant evolutions of crystal structure and electronic properties are quite different [4,7,8,20]. A detailed comparative study on the dependence of superconducting transition temperature on external parameters in $2H$-TaS_2 is still absent. In this regard, it is essential to clarify the comparative effects of sample quality and hydrostatic pressure on superconducting phase diagrams.

High pressure is an effective method to manipulate crystal structures and/or electronic properties. For superconductors, the pressure dependence of several superconducting parameters provides useful information on superconducting pairing mechanisms. Different from chemical doping, physical pressure is clean and doesn't introduce any excessive disorder and can reveal intrinsic pressure effect of physical phenomena [21,22]. In this work, we report the effects of disorder and hydrostatic pressure on CDW and SC of $2H$-TaS_2. Along with pressure-induced collapse of CDW for those crystals in the clean limit (low disorder level), the domelike dependence of T_c is accompanied by a sizable reduction in temperature exponent and nearly one order increase in the quadratic temperature coefficient of normal-state resistivity near P_c. However, the maximal T_c^{max} is reduced by disorder scatterings for those crystals with high disorder level where impurity scattering destroys superconducting pairing.

II. EXPERIMENTAL METHODS

Single-crystal $2H$-TaS_2 (nos. $S1$–$S8$) was grown with the chemical vapor transport method and checked again by using x-ray diffraction; the analysis results show that their cell parameters are basically the same except the slight broadening of diffraction peaks for no. $S8$ [5,20]. At AP, temperature dependence of electrical transport $\rho(T)$ was measured for all the samples on the Quantum Design Physical Property Measurement System (1.8 K $\leqslant T \leqslant$ 400 K, $0 \leqslant H \leqslant$ 9.0 T). Under pressures, the piston-cylinder pressure cell (PCC) and the palm-type cubic anvil pressure cell (CAC) were employed to measure electrical resistivity and ac magnetic susceptibility for selected single-crystal $2H$-TaS_2. Here, PCC has two opposed anvils but can provide high hydrostatic pressure because Glycerol as the pressure transmitting medium (PTM) remains liquid below 3.0 GPa; CAC apparatus generates hydrostatic pressures with multiple-anvil geometry; it could be achieved by triaxial compression and liquid PTM even when PTM solidifies under higher pressures; bulk Pb is used as pressure manometer and glycerol as PTM [21,22]. Electrical resistivity is measured by four-probe method with the current parallel to the ab-plane and the field parallel to the c axis of crystals. AC magnetic susceptibility data were collected at a fixed frequency with AC magnetic field parallel to the *ab* plane of crystals. In this work, the experiments were performed on a ^{4}He refrigerated cryostat (1.4 K $\leqslant T \leqslant$ 295 K and 0 T $\leqslant H \leqslant$ 9 T).

III. RESULTS AND DISCUSSION

In Fig. 1, we first examine the dependence of T_{CDW} and superconducting properties on sample quality at AP. As in Fig. 1(a), the normalized temperature dependence of resistivity $\rho(T)$ data is plotted for all the single-crystal $2H$-TaS_2 (nos. $S1$–$S8$). For nos. $S1$ and $S2$, $\rho(T)$ shows clear metallic behavior in the whole temperature range with a pronounced shoulder near 78 K, which just corresponds to the reported ICCDW phase transition [15,20], while for nos. $S3$–$S7$, the ICCDW phase transition temperature broadens up and slightly shifts down to lower temperatures, which is accompanied by a resultant decrease in the residual resistivity ratio (RRR) (defined as $\rho_{300 K}/\rho_0$) and an increase in the residual resistivity ρ_0 compared to those of no. $S1$; however, for no. $S8$, the ICCDW phase transition cannot be detected with further decrease of the RRR value. These results indicate that long-range CDW phase transition of $2H$-TaS_2 is suppressed with the decrease of the RRR value and collapsed completely above
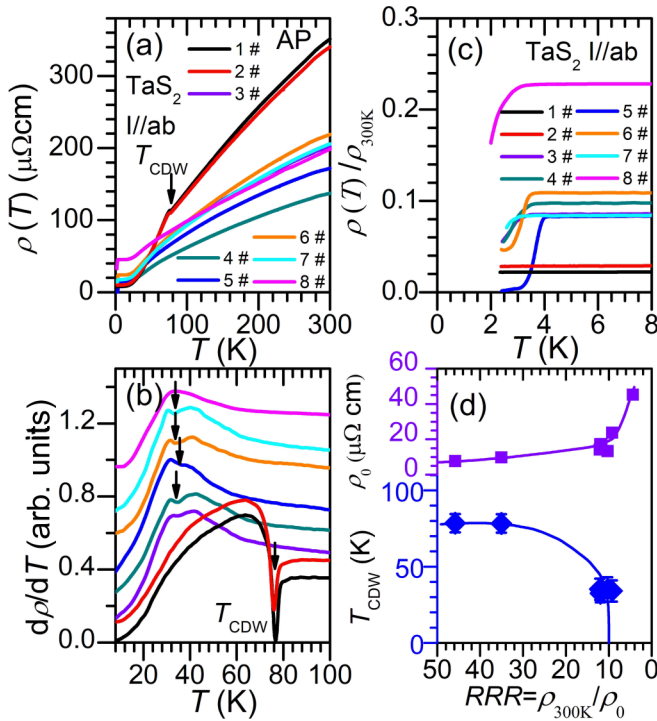
FIG. 1. (a) Temperature dependence of electrical resistivity $\rho(T)$ for single-crystal $2H$-TaS$_2$ (nos. $S1$–$S8$) with the measuring current parallel to the ab plane of crystals; the back arrow indicates IC-CDW phase transition of $2H$-TaS$_2$ and is marked by T_{ICCDW}; (b) temperature dependence of the derivative $d\rho(T)/dT$ is plotted and T_{CDW} is defined as the temperature with the $d\rho(T)/dT$ maximum; for comparison, the absolute $d\rho(T)/dT$ was shifted vertically; (c) the enlargement of low-T $\rho(T)/\rho(300\,\mathrm{K})$ ($0 \leqslant T \leqslant 8\,\mathrm{K}$), where $\rho(300\,\mathrm{K})$ represents electrical resistivity at 300 K. The dependence of characteristic parameters on the residual resistivity ratio RRR [$= \rho(300\,\mathrm{K})/\rho_0$]; (d) the residual resistivity ρ_0; ρ_0 was estimated by fitting the formula $\rho = \rho_0 + AT^n$ and ICCDW phase transition temperature T_{ICCDW}. The dashed lines indicate the changing tendency.

critical values. Accompanying this, it is found that T_{CDW} and the superconducting transition show sample dependence with different RRR and ρ_0. The dependence of characteristic parameters ρ_0 and T_{CDW} on the RRR is plotted and compared in Fig. 1(d). Here, T_{CDW} was defined as the peak temperature of the derivation $d\rho(T)/dT$ in Fig. 1(b), however, there is no zero resistivity state in $2H$-TaS$_2$ (nos. $S1$–$S8$) in our measured temperature range. Several clear features can be summarized as follows: With reducing the RRR value from 45.8 to 10.2, ρ_0 increases nearly three times in magnitude and T_{CDW} is reduced from 78 K to ~ 41 K gradually and accompanied by a quick increase in the superconducting phase transition temperature. However, with further reducing the RRR value to 4.4, the magnitude of ρ_0 quickly increases another three times and long-range CDW phase transition cannot be detected; all these support the competition of CDW and SC. In addition, these features indicate the increase of the residual resistivity and RRR (from no. $S1$ to no. $S8$) is closely associated with T_{CDW}; and it thus can be regarded as a criterion of sample quality and/or disorder which strongly depends on external factors such as the sintered temperatures and lattice mismatches [20].

In detail, different disorder levels can be conjectured by comparing RRR and the residual resistivity ρ_0 compared to those of no. $S1$ in the clean limit (low disorder level). This regular change is reflected in the change of sample quality such as disorder level. There are slight differences in the experimental conditions such as the annealing temperatures and sintering time. Similar behaviors have been reported in other CDW materials such as $2H$-TaSe$_{2-x}$S$_x$ where the evolution of the superconducting state was thought to originate from disorder scatterings rather than chemical pressure effect and band fillings [20]. The present results support the conclusions that disorder destabilizes long-range CDW and enhances SC. Moreover, the plot of T_{CDW} vs ρ_0 is shown in Fig. S1 of the Supplemental Material [23]; with increasing ρ_0, T_{CDW} decreases with the enhanced SC, which seems contrary to Anderson's theory if ignoring the ICCDW phase [24]; however, in this process, disorder scattering and the melting of CDW are two factors affecting SC, and the latter dominates the change of the superconducting state with the increase of disorder scattering at AP.

To study the effects of hydrostatic pressure and sample quality on phase diagrams of CDW and SC, we chose two representative single-crystal $2H$-TaS$_2$ for comparison: namely, no. $S1$ (RRR ~ 45.8, $\rho_0 \sim 7.7\,\mu\Omega\,\mathrm{cm}$) in the clean limit (low disorder level) and no. $S8$ (RRR ~ 4.4, $\rho_0 \sim 45.3\,\mu\Omega\,\mathrm{cm}$) in the dirty limit (high disorder level), respectively. As in Figs. 2(a), 2(b), and S2 [23], $\rho(T)$ were measured under various pressures for no. $S1$. Room-temperature resistivity at 12.5 GPa reduces to one-half that at AP. On cooling from 300 K, $\rho(T)$ shows metallic behavior and the ICCDW phase transition is shifted down to ~ 37.1 K at 5.5 GPa and then cannot be detected under higher pressures. The evolution of T_c and T_{CDW} are determined in Figs. 2(d), 2(e), and S2 [23]. It is sure that the applied pressure collapses long-range CDW at a certain critical pressure P_c. With these characteristics, superconducting properties change greatly. As shown in Figs. 2(g) and 2(h), on cooling, a superconducting phase transition appears and increases with pressure; T_c increases monotonously from 2.30 K at 0.16 GPa to 5.7 K at 2.0 GPa and the maximum superconducting transition temperature ~ 9.15 K near a critical pressure of 6.50 GPa, and then decreases slightly down to 8.85 K with further increasing pressure up to 12.5 GPa. Pressure dependence of T_{CDW} and T_c is plotted in Fig. 4(a). It is found that a "domelike" superconducting state is closely adjacent to the CDW boundary and the T_c value reaches the maximum at the critical pressure P_c where the long-range CDW collapses as indicated in electrical resistivity. This indicates strong competition between CDW and SC [10,16]. Meanwhile, for no. $S8$ in the dirty limit (high disorder level), no CDW phase transition can be detected in $\rho(T)$ as in Figs. 2(c), 2(f), and 2(i). Low-T $\rho(T)$ shows a slightly drop at 3.2 K at AP. With increasing the pressure, low-T resistivity drop is enhanced by nearly four times in magnitude compared to that at AP, and the T_c value increases monotonously to 6.43 K at 7.0 GPa and then decreases to 5.60 K at 11.5 GPa. It is quite strange that $T_c(P)$ shows a broad domelike dependence although there is no long-range CDW, and the maximum T_c^{max} is about 3 K lower than that of no. $S1$, which should be closely correlative to impurity scatterings [20]. It is unclear whether there is some undetected CDW in resistivity.
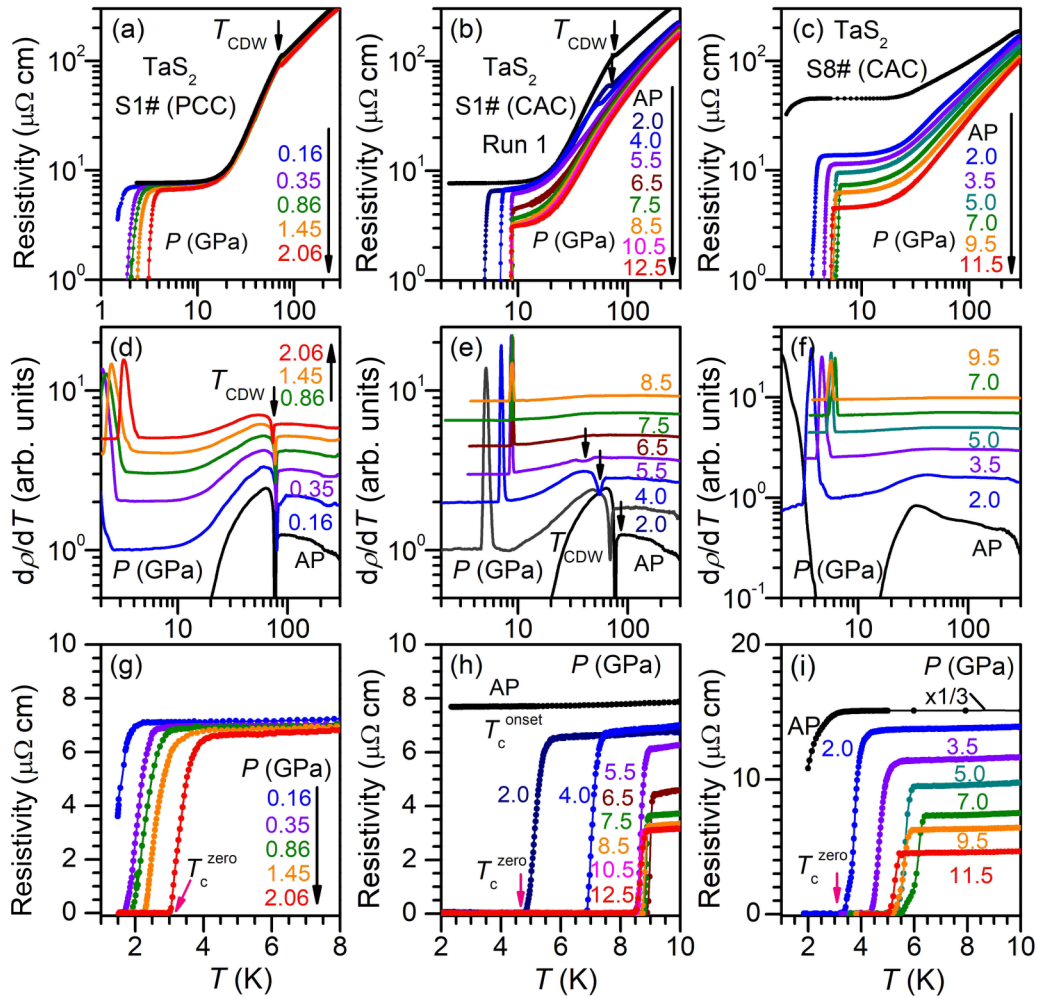
FIG. 2. $\rho(T)$ under various pressures with the current parallel to *ab* plane of crystals: (a) $2H$-TaS_2 (no. $S1$) in PCC up to 2.06 GPa; (b) $2H$-TaS_2 (no. $S1$) in CAC apparatus up to 12.5 GPa for run 1; (c) $2H$-TaS_2 (no. $S8$) in CAC up to 11.5 GPa. (d)–(f) Temperature dependence of $d\rho/dT$ for nos. $S1$ and $S8$, respectively. (g)–(i) The enlargement of low-T $\rho(T)$; the black and red arrows indicate T_{ICCDW} and zero resistivity temperature T_c^{zero}, respectively. "CAC" is short for the cubic anvil pressure cell and "PCC" is the piston cylinder pressure cell.

Temperature dependence of high-pressure magnetic susceptibility was measured for no. $S1$ and superconducting shielding volume $4\pi\chi_v(T)$ was estimated by comparing its diamagnetic signal of samples with that of reference Pb as in Fig. 3(a) [3]. As we know, magnetic susceptibility under high pressure is challenging. It is thought that AC susceptibility is achieved by testing bulk characteristics of superconductors, and thus is used as the criterion to judge whether it is bulk SC or not. From this point of view, we can safely describe the evolution of susceptibility under pressure to obtain important superconducting parameters including the evolution of superconducting volume ratio and superconducting transition temperature. We can note, with increasing the pressure, that $4\pi\chi_v(2\,K)$ quickly increases from 58.8% at 2.0 GPa, and then to 87.8% near 6.0 GPa, and then retains a constant value up to 10 GPa, which suggests that more electrons participate in superconducting pairings. However, the maximum of the volume AC susceptibility isn't 1, which should be reasonable considering the usual error (5–10%) of AC susceptibility under high pressure but it does not affect the judgment of bulk SC; combined the above resistivity results, it can be

concluded that $2H$-TaS_2 transits from ICCDW into bulk SC by pressure. In addition, as in Figs. 3(b) and 3(c), the obtained superconducting transition temperature T_c^M, where $4\pi\chi_v(T)$ decreases to one-half of the saturation values at lower temperatures, is basically equal to T_c values determined from the zero resistivity state of a superconducting phase transition in $\rho(T)$. These results not only confirm bulk SC of $2H$-TaS_2, but also show that magnetic susceptibility data under high pressure are reliable. Besides, both T_c and $4\pi\chi_v(2\,K)$ exhibit consistent pressure dependence and reach the maximum at the same critical pressures, which implies that the domelike SC is attributed to pressure-induced collapse of long-range CDW [6,7,10]. However, it is possible that some short-range CDWs above P_c coexist with SC because they cannot be detected in resistivity [11,25].

To interpret domelike superconducting diagrams, normal-state resistivity just above T_c was analyzed quantitatively by an empirical formula $\rho = \rho_0 + AT^n$, where ρ_0 represents the residual resistivity, the temperature coefficient A and temperature exponent n are associated with the density of states at Fermi level and the inelastic electron scatterings, respectively.
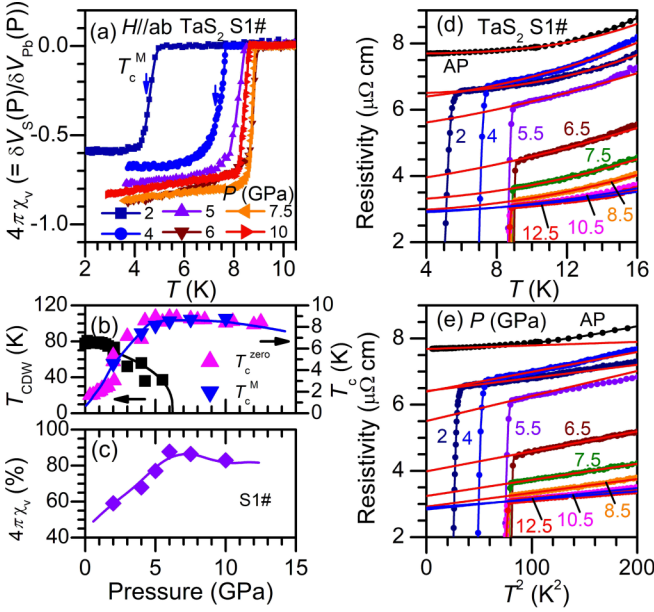
FIG. 3. (a) Temperature dependence of superconducting shielding volume $4\pi\chi_v(T)$ at a fixed frequency under a modulation AC magnetic field which is parallel to ab plane of crystals for no. $S1$. Blue arrows show superconducting transition temperature T_c^M where $4\pi\chi_v(T)$ decreases to one-half of the saturation values at lower temperatures. Pressure dependence of the characteristic temperatures: (b) T_{CDW}, T_c^M, and T_c^{zero}; (c) $4\pi\chi_v$; the dashed lines indicate changing trends. Two different fittings are performed by $\rho = \rho_0 + AT^n$: the polynomial fitting for $T < 20\,K$ gives ρ_0 and n and (d) the linear fitting for $n = 2$ to low-temperature data give the value of parameter A. The solid lines across the data indicate the fitting results.

FIG. 4. Temperature-pressure phase diagram for (a) $2H$-TaS$_2$, no. $S1$ and (b) $2H$-TaS$_2$, no. $S8$, respectively. The changing colors describe the tendency of resistivity. The data points of Cu interaction are from Refs. [29,30]. The black lines are the fitting results by $T_{ICCDW} = T(AP)(1\text{-}P/P_c)^\beta$, where the $T(AP)$, the P_c, and the β represent the T_{ICCDW} at AP, the critical pressure where T_{CDW} reduces to zero, and the exponent n characterizing the suppression of parameters, respectively. The red lines represent the changing trends in (a) and (b). Pressure dependence of parameters in the same scales for nos. $S1$ and $S8$: (c) ρ_0, (d) A, (e) n, and (f) T_c. The lines across the data show the changing trends.

As in Figs. 3(d), 3(e), and S3 [23], the polynomial fitting for $T < 20\,K$ gives ρ_0 and n and the linear fitting for $n = 2$ to low-temperature data gives the parameter A. Temperature-pressure phase diagrams are plotted in Figs. 4(a) and 4(b) for nos. $S1$ and $S8$, respectively. The colors in the phase diagrams reflect the changes of electrical resistivity in the same scales. T_{CDW} of no. $S1$ decreases with increasing the pressure and reduces to zero at $P_c \sim 6.24(5)\,GPa$, while for no. $S8$, the ICCDW phase transition cannot be detected in resistivity because the enhanced disorder scatterings destroy long-range CDW. To describe the evolution of CDW, pressure dependence of ICCDW can be well fitted according to the previous reports by the model $T_{ICCDW} = T(AP)(1\text{-}P/P_c)^\beta$, where $T(AP)$, P_c, and β represent the T_{ICCDW} at AP, the critical pressure for the collapse of CDW order, and the pressure exponent which describes the suppression of CDW, respectively [3,8,9]. It has been proved to be reliable in understanding the evolution of CDW in various materials. Using the data, $T(AP)$, P_c and β are determined to be 79.49 K, 6.24(5) GPa, and 0.374(2) for no. $S1$, respectively. However, we must note that the critical pressure should be a range of pressure values, and the acquired critical pressure $P_c \sim 6.24(5)\,GPa$ is only a mathematical fitting result; besides, P_c is found to be close to other reported ones of 7.3 GPa [18], 8.50 GPa [17], 8.70 GPa [19], but the β [0.374(2)] is smaller than those of typical TMDC materials [8,9]. These features imply that CDW order should be more
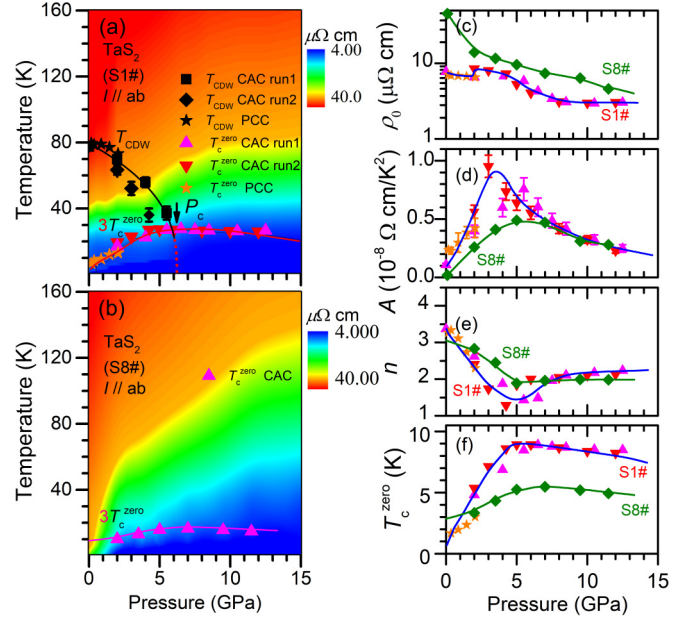
sensitive to hydrostatic pressure and CDW correlation lengths are different depending on distinct pressure environments.

In Figs. 4(c)–4(g), pressure dependence of ρ_0, A, n, and T_c^{zero} are plotted and compared. For no. $S1$, both ρ_0 and A increase and reach the maximum near 6.50 GPa and decrease with further increasing pressure, which is a positive correlation with the domelike pressure dependence of T_c; more interestingly, the A value shows one order enhancement at P_c, which is evidence for the increase of density of states at the Fermi level and is consistent with the above results of magnetic susceptibility [26,27]. Accompanying this, the temperature exponent n reduces quickly from $\sim$3.36 at AP to $\sim$1.29(2) at P_c and increases up to nearly constant $\sim$2.10(4) above 7.5 GPa. It is believed that non-Fermi-liquid behavior appears with pressure-induced collapse of CDW near P_c and recovers to Fermi-liquid behavior. For a Fermi liquid, the departures from $n = 2$ could be interpreted to be the changes of electron correlations. Temperature exponent n shows a "trough" pressure dependence and is similar to that of $1T$-TiSe$_2$ with a sizeable suppression of the n values near P_c. These characteristics were attributed to CDW critical fluctuations [10]. Combined with the results, CDW quantum criticality can be concluded with strong competitions between CDW and SC at P_c [10,26,27].

For no. $S8$, ρ_0 reduces monotonically by one order of magnitude up to 11.5 GPa, more quickly than that of no. $S1$. T_c
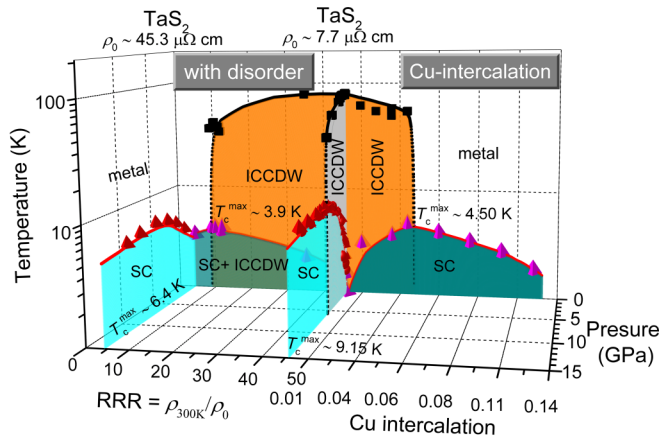
FIG. 5. Phase diagram of single-crystal $2H$-TaS$_2$ in the temperature, pressure, the RRR value [defined as $\rho(300\,\text{K})/\rho_0$], and Cu intercalation. The dashed and solid lines indicate changing trends. The $T_c^{\max}$ is the highest superconducting phase transition temperature. "ICCDW" represents the incommensurate CDW phase transition and "SC" is the superconductivity, respectively.

exhibits domelike pressure dependencies with $T_c^{\max} \sim 6.43$ K at 6.50 GPa; meanwhile, the enhancement in the A value is just one-half in magnitude compared to that of no. $S1$ and covers broad pressure windows; it is found that similar features in no. $S1$ are unapparent and even vanish in no. $S8$ by contrast. One reason is that the enhanced disorder scatterings broaden energy bands and cause the reduction in the $T_c^{\max}$; the reduction in T_c with further increasing pressure above P_c could be attributed to the weakness of superconducting pairing strength by impurity scattering [20]. Meanwhile, the T_c of no. $S8$ shows broad domelike pressure dependence although there is no long-range CDW phase transition as shown in no. $S1$. We should also note the fact that long-range CDW could become short range in strongly disordered crystals and cannot be detected in resistivity data. As suggested by Cho *et al.* [28], with increasing the disorder in NbSe$_2$, there is a gradual crossover from long-range CDW into a short-range one by measuring the x-ray diffraction. This is the possible reason for the absence of CDW phase transition in the resistivity data. It is thought that the competition of short-range CDW and SC under pressure may lead to the broad humplike $T_c(P)$.

Figure 5 shows the temperature-pressure-composition phase diagram of $2H$-TaS$_2$. At AP, with increasing the disorder and Cu intercalation, T_{CDW} reduces and vanishes at some critical values; as a result, T_c rises and gets the maximum $T_c^{\max}$ of 3.90 and 4.70 K at the optimal doping level, respectively. Similarly, the domelike pressure dependence of T_c is achieved at the expense of CDW collapse near $P_c \sim 6.50$ GPa. But $T_c^{\max}$ shows strong sample dependence: $T_c^{\max} \sim 9.15(2)$ K for no. $S1$ in the clean limit (low disorder level) is about 3 K higher than ~ 6.42 for no. $S8$ with enhanced disorder. And $T_c^{\max} \sim 9.15(2)$ K is nearly two times higher than that at AP (4.70 K). These results indicate that hydrostatic pressure can optimize band structures and electronic correlations to a great extent through lattice contraction and that disorder scattering could enhance SC through the suppression of CDW, but excessive disorder weakens superconducting pairing strength and restricts the further increase of $T_c^{\max}$.

Finally, we discuss several important issues. The first is the reason why T_c exhibits similar domelike dependence by element doping, disorder, Cu intercalation, and high pressure although lattice parameters and electronic properties are changed differently [16–20,29,30]. Usually, the disorder destroys long-range CDW order through lattice distortions and broadens electronic bands which might partially fill the CDW energy gap [20], while the Cu-intercalation enlarges the c axis of crystals and weakens van der Waals interaction; its main result is thought to be the increase of carrier concentration and electron-phonon coupling strength [29,30]; T_c reduces with more impurity scatterings after the collapse of long-order CDW order [4]. Differently, without the influence of disorder, hydrostatic pressure causes lattice contraction and phonon instabilities; T_c enhances as the result of the increase in the density of state at Fermi level and electron-phonon coupling [16–19]; above P_c, the reduction of T_c might be attributed to the decrease in the density of state at Fermi level with pressure-induced band broadening and overlaps [19]. The second one is a large difference in critical pressure P_c. As reported, P_c can span a wide pressure range from 7.3 to 17 GPa, which is closely associated with pressure environments, sample quality, as well as the measurement of pressure [16–19]. In this work, pressure at low temperature is extrapolated by susceptibility of the superconducting phase transition of lead, which eliminates the error to the maximum extent. Moreover, CAC apparatus generates hydrostatic pressure with multiple-anvil geometry and liquid glycerol as the PTM with higher solidification pressures [21,22]. Thus, the reliability of P_c and the measured pressures in this paper are more accurate than other studies. Meanwhile, we note that there are not only larger differences in P_c but also in $T_c^{\max}$, which cannot be explained alone by an inaccurate reading of pressure. It should be more emphasized that the other studies must have been performed on samples with different disorder levels, which might explain the above differences.

The third is the interplay of CDW and SC; in one report, T_c continues to increase and reaches its maximum at 11.5 GPa, which doesn't support simple competition of CDW and SC [18], but in other cases, pressure dependence of T_c values, which could be determined from Raman spectroscopy and magnetic susceptibility, gets its maximum accompanying the collapse of CDW, which indicates the strong competition of CDW and SC [17,19]. In this work, our results support the conclusion of strong competition between CDW and SC by regulating structural and electrical properties by continuous pressurization in CAC apparatus. The last question is the superconducting properties of $2H$-TaS$_2$ under pressure. According to the temperature/magnetic field dependence of electrical resistivity in Fig. S4 [23], T_c moves to lower temperatures owing to the magnetic pair-breaking effect and the superconducting transition width broadens with increasing the fields which can be attributed to magnetic flux creep effect. These features suggest that $2H$-TaS$_2$ can be classified as a type-II superconductor. Besides, we note that $T_c^{\max}$ (9.15 K) under pressure is nearly two times higher than those of Cu-intercalated $2H$-TaS$_2$ at AP [29,30], which indicates that pressure optimizes energy bands and enhances T_c to the maximum. These features could be reflected by the differences in normal-state ρ_0, which indicates different properties such as

carrier concentration and disorder degree [29–31]. To clarify this, more theoretical investigations are required.

IV. CONCLUSION

In summary, the effects of disorder and hydrostatic pressure on superconducting phase diagrams of $2H$-TaS$_2$ were studied comparatively. T_c exhibits domelike pressure dependence for crystals in clean limit (low disorder level) and reaches the maximum of $\sim$9.15 K at a critical pressure P_c, which is accompanied by a sizable reduction in the temperature exponent and one order enhancement in the temperature coefficient of normal-state resistivity near P_c, while for those crystals in the dirty limit (high disorder level), the pressure dependence of $T_c(P)$ and n broaden up and become less apparent in comparison with clean crystals. Our results suggest that disorder scattering and the melting of the CDW are two factors affecting SC, and the melting of the CDW, not disorder scattering, dominates the T_c with pressure below P_c; however, superconducting pairing strength is weakened by impurity scattering above P_c.

[1] G. Grüner, Rev. Mod. Phys. **60**, 1129 (1988).

[2] A. H. Castro Neto, Phys. Rev. Lett. **86**, 4382 (2001).

[3] B. S. Wang, Y. Liu, K. Ishigaki, K. Matsubayashi, J.-G. Cheng, W. J. Lu, Y. P. Sun, and Y. Uwatoko, Phys. Rev. B **95**, 220501(R) (2017).

[4] Y. Liu, R. Ang, W. J. Li, W. H. Song, L. J. Li, and Y. P. Sun, Appl. Phys. Lett. **102**, 192602 (2013).

[5] J. A. Wilson, F. J. Di Salvo, and S. Mahajan, Phys. Rev. Lett. **32**, 882 (1974).

[6] B. Sipos, A. Kusmartseva, A. Akrap, L. F. H. Berger, and E. Tutis, Nat. Mater. **7**, 960 (2008).

[7] E. Morosan, H. W. Zandbergen, B. S. Dennis, J. W. G. Bos, Y. Onose, T. Klmczuk, A. P. Ramirez, N. P. Ong, and R. J. Cava, Nat. Phys. **2**, 544 (2006).

[8] B. S. Wang, Y. Liu, X. Luo, K. Ishigaki, K. Matsubayashi, W. J. Lu, Y. P. Sun, J.-G. Cheng, and Y. Uwatoko, Phys. Rev. B **97**, 220504(R) (2018).

[9] Y. I. Joe, X. M. Chen, P. Ghaemi, K. D. Finkelstein, G. A. de la Pena, Y. Gan, J. C. T. Lee, S. Yuan, J. Geck, G. J. MacDougall, T. C. Chiang, S. L. Cooper, E. Fradkin, and P. Abbamonte, Nat. Phys. **10**, 421 (2014).

[10] A. F. Kusmartseva, B. Sipos, H. Berger, L. Forro, and E. Tutis, Phys. Rev. Lett. **103**, 236401 (2009).

[11] A. Kogar, G. A. de la Pena, Sangjun Lee, Y. Fang, S. X.-L. Sun, D. B. Lioi, G. Karapetrov, K. D. Finkelstein, J. P. C. Ruff, P. Abbamonte, and S. Rosenkranz, Phys. Rev. Lett. **118**, 027002 (2017).

[12] R. Ang, Y. Miyata, E. Ieki, K. Nakayama, T. Sato, Y. Liu, W. J. Lu, Y. P. Sun, and T. Takahashi, Phys. Rev. B **88**, 115145 (2013).

[13] H. W. Myron and A. J. Freeman, Phys. Rev. B **11**, 2735 (1975).

[14] C. A. Balseiro and L. M. Falicov, Phys. Rev. B **20**, 4457 (1979).

[15] J. M. E. Harper, T. H. Geballe, and F. J. Disalvo, Phys. Rev. B **15**, 2943 (1977).

[16] D. C. Freitas, P. Rodière, M. R. Osorio, E. Navarro-Moratalla, N. M. Nemes, V. G. Tissen, L. Cario, E. Coronado, M. García-Hernández, S. Vieira, M. Núñez-Regueiro, and H. Suderow, Phys. Rev. B **93**, 184512 (2016).

[17] R. Grasset, Y. Gallais, A. Sacuto, M. Cazayous, S. Manas-Valero, E. Coronado, and M.-A. Measson, Phys. Rev. Lett. **122**, 127001 (2019).

[18] X.-M. Zhao, K. Zhang, Z.-Y. Cao, Z.-W. Zhao, V. V. Struzhkin, A. F. Goncharov, H.-K. Wang, A. G. Gavriliuk, H.-K. Mao, and X.-J. Chen, Phys. Rev. B **101**, 134506 (2020).

[19] Y. Kvashnin, D. VanGennep, M. Mito, S. A. Medvedev, R. Thiyagarajan, O. Karis, A. N. Vasiliev, O. Eriksson, and M. Abdel-Hafiez, Phys. Rev. Lett. **125**, 186401 (2020).

[20] L. J. Li, X. Y. Deng, Z. Wang, Y. Liu, M. Abeykoon, E. Dooryhee, A. Tomic, Y. N. Huang, J. B. Warren, E. S. Bozin, S. J. L. Billinge, Y. P. Sun, Y. M. Zhu, G. Kotliar, and C. Perovis, NPG Quantum Mater. **2**, 11 (2017).

[21] N. Mori, H. Takahashi, and N. Takeshita, High Pressure Res. **24**, 225 (2004).

[22] J.-G. Cheng, K. Matsubayashi, S. Nagasaki, A. Hisada, T. Hirayama, M. Hedo, H. Kagi, and Y. Uwatoko, Rev. Sci. Instrum. **85**, 093907 (2014).

[23] See Supplemental Material at http://link.aps.org/supplemental/10.1103/PhysRevB.103.224509 for the temperature dependence resistivity and the upper critical fields at 7.5 and 10 GPa, respectively.

[24] P. W. Anderson, J. Phys. Chem. Solids **11**, 26 (1959).

[25] J. Joshi, H. M. Hill, S. Chowdhury, C. D. Malliakas, F. Tavazza, U. Chatterjee, A. R. Hight Walker, and P. M. Vora, Phys. Rev. B **99**, 245144 (2019).

[26] H. Q. Yuan, F. M. Grosche, M. Deppe, G. Sparn, C. Geibel, and F. Steglich, Phys. Rev. Lett. **96**, 047008 (2006).

[27] Z. Ren, L. V. Pourovskii, G. Giriat, G. Lapertot, A. Georges, and D. Jaccard, Phys. Rev. X **4**, 031055 (2014).

[28] Kyuil Cho, M. Kończykowski, S. Teknowijoyo, M. A. Tanatar, J. Guss, P. B. Gartin, J. M. Wilde, A. Kreyssig, R. J. McQueeney, A. I. Goldman, V. Mishra, P. J. Hirschfeld, and R. Prozorov, Nat. Commun. **9**, 2796 (2018).

[29] X. D. Zhu, Y. P. Sun, S. H. Zhang, J. L. Wang, L. J. Zou, L. E. Delong, X. B. Zhu, X. Luo, B. S. Wang, G. Li, Z. R. Yang, and W. H. Song, J. Phys: Condens. Matter **21**, 145701 (2009).

[30] K. E. Wagner, E. Morosan, Y. S. Hor, J. Tao, Y. Zhu, T. Sanders, T. M. McQueen, H. W. Zandbergen, A. J. Williams, D. V. West, and R. J. Cava, Phys. Rev. B **78**, 104520 (2008).

[31] X. D. Zhu, Y. P. Sun, X. B. Zhu, X. Luo, B. S. Wang, G. Li, Z. R. Yang, W. H. Song, and J. M. Dai, J. Cryst. Growth **311**, 218 (2008).